Mechanistic Insights into the Rhodium-Catalyzed Aryl C–H Carboxylation

DeGuang Liu*

Hefei National Laboratory for Physical Sciences at the Microscale, CAS Key Laboratory of Urban Pollutant Conversion, Anhui Province Key Laboratory of Biomass Clean Energy, iChEM, University of Science and Technology of China, Hefei, 230026, China.

ABSTRACT: The recently reported Rh(II)-catalyzed direct C-H bond activation and lactonization of 2-arylphenols uncovers an attractive strategy to prepare coumarin derivatives with high site-selectivity. Motivated by the mechanistic ambiguity (on the origin of the site-selectivity and the details for lactonization *etc.*), we conducted a detailed mechanistic study of the rhodium-catalyzed lactonization of 2-arylphenols with density functional theory (DFT) calculations. The results suggest that the reaction occurs via the coordination exchange, C-H bond activation, carboxylation, protonation and lactonization steps. The rate-determining step is the carboxylation step, in which CO_2 favorably inserts into the Rh-C bond (instead of the more nucleophilic Rh-O bond). The protonation step after carboxylation is critical, which makes the subsequent CO_2-assisted lactonization feasible. Interestingly, the corresponding pKa value of the base can reasonably predict the reaction energy barrier of the C-H bond activation step. The calculations will provide insights and suggestions for the development and advancement of the subsequent C-H bond activation carboxylation reaction.

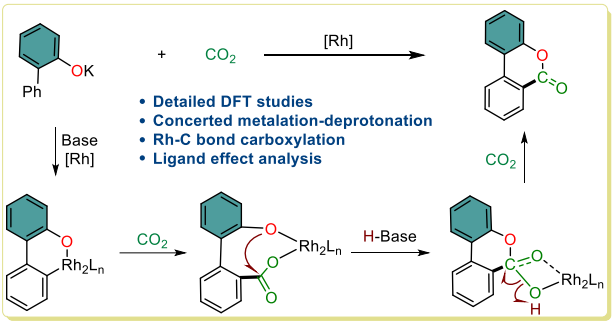

KEYWORD: DFT calculations, 2-Arylphenols, C-H bond activation, Carboxylation

INTRODUCTION

The C1 building block of CO_2 has recently become a highly attractive synthon for its abundance, nontoxicity and renewability.[1] Among the various CO_2-transformation strategies, the synthesis of valuable carboxyl derivatives via direct activation of the C-H bond with a subsequent carboxylation represents one of the most practical one.[2] Specifically, such strategy has been successfully utilized to prepare aromatic carboxylic acids, which are essential building blocks in pharmaceuticals of nonsteroidal anti-inflammatory drugs.[3] Nevertheless, due to the relatively low reactivity of CO_2, the transformation of aryl C-H bonds into highly strong nucleophiles, such as organozinc compounds, organoboronic esters, and allylstannanes are always necessary (Scheme 1a).[4] The requisite of the stoichiometric organometallic reagents greatly limited the functional group tolerate. In this context, the direct aryl C-H bond activation-carboxylation (with CO_2) could be more

appealing with respect to the atomic economy and applicability, but is still challenging in these years. Besides, the base-promoted Kolbe-Schmitt reaction of phenol derivatives (Scheme 1b)[5] and the aluminium-promoted Friedel-Crafts type of carboxylation (Scheme 1c)[6] occur dominantly on the most nucleophilic site of the arene substrates, while the carboxylation on the less-nucleophilic sites is yet to be developed. An interesting progress was recently accomplished by Li and co-workers, in which carboxylation occurs exclusively on the less nucleophilic site of the inactivated phenyl ring, instead of the more nucleophilic site of the phenol ring (Scheme 1d).[7]

Scheme 1. Selected examples for C-H carboxylation of 2-(hetero)arylphenols with CO_2.

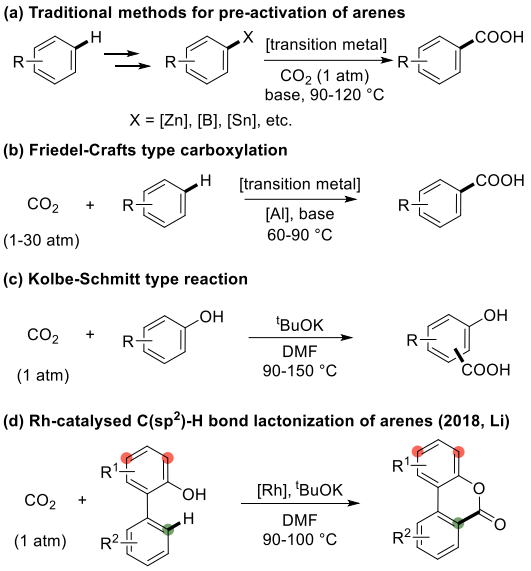

Li and co-workers suggested a mechanism for the reaction in Scheme 1d.[7] As shown in Scheme 2, the potassium alkoxide substrate (**1aK**) enters the catalytic cycle through ligand exchange to generate the intermediate **II**. Then the alkali-assisted C-H bond activation step occurs to obtain the metallacycle species **III**. Insertion of CO_2 into the Rh-C bond then generates the intermediate **IV**. Subsequently, lactonization is achieved through a comprehensive ligand exchange and C-O bond formation steps, associating with the regeneration of **I**. In the context of the proposed mechanism, one of the most intriguing mechanistic question is the origin of the preferential CO_2 insertion into the less nucleophilic Rh-C bond, instead of the more nucleophilic Rh-O bond. Meanwhile, the complexity of the lactonization step promotes us to explore the details of the elementary steps (such as the effect of base), and the driving force.

Herein, density functional theory (DFT) calculations were conducted to explore the mechanism of the C-H carboxylation shown in Scheme 1d. The calculations corroborates Li's mechanistic proposal on the prior ligand exchange, C-H bond cleavage and nucleophilic steps. Nevertheless, instead of **1aK** mediated C-H activation, potassium hemicarbonate ($^tBuOCO_2K$, generated by the carboxylation of ^tBuOK) could remarkably accelerate the C-H activation via a concerted metalation-deprotonation (CMD) mode. Meanwhile, the Rh-O carboxylation is competitive with the Rh-C carboxylation. The former is kinetically favored, but thermodynamically disfavored (i.e. reversible elementary step). Therefore, the Rh-C carboxylation occurs preferentially to form the metallacycle intermediate (type **IV'**) due to the thermodynamic advantages. After that, lactonization occurs via a cascade protonation, cyclization and ligand exchange steps. Finally, the carboxylation and a subsequent dissociation of $KHCO_3$ occurs to regenerate the intermediate type **II**. To this end, except

for the first catalytic cycle (starts with type **I**), all the subsequent catalytic cycle start with the type **II**. The base ^{t}BuOK plays two pivotal roles: facilitate the C-H metalation (in the form of potassium hemicarbonate); and mediate the catalyst regeneration (in the form of **1aK**).

Scheme 2. The tentative catalytic cycle.

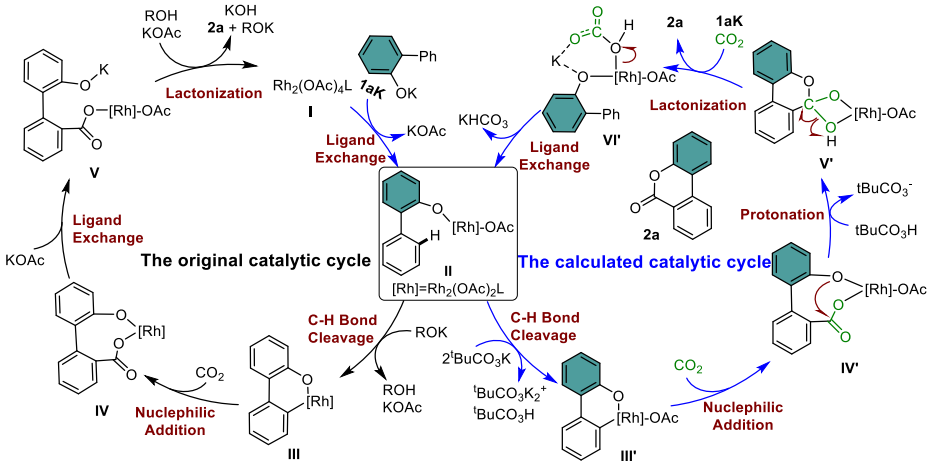

Computational Methods: All calculations were performed with Gaussian 16, Rev. C01 package.[8] The B3LYP[9] functional, associated with the Grimme dispersion correction (GD3BJ),[10] was used for geometry optimization of all structures. This functional has been used in similar Rh-catalyzed coupling reaction systems before.[11] The basis set SDD[12] (including related pseudopotential) was employed on rhodium and the 6-31G(d)[13] was employed on other elements. Frequency analysis was performed at the same level of theory with the geometry optimization to confirm that the optimized structures are local minima or transition states, and to gain the thermal correction of Gibbs free energy. The consistency of the X-ray single-crystal data of the isolated intermediates with the optimized structures verifies the optimization methods (Figure S1).[7] In this context, single-point energy calculations were conducted on the basis of optimized structures, and with the M06[14] functional, including Grimme dispersion correction (GD3). The combination of SDD (related pseudopotential included) and the 6-311+G(d,p) basis set were employed on rhodium and the other elements, respectively. The solvent effects were taken into account by employing the SMD[15] (N, N-dimethylformamide) solvation model. The intrinsic reaction coordinate (IRC)[16] calculations were performed to ensure that the transition state connects the correct reactants and products. All energies in this study are Gibbs free energy and given in kcal/mol. The wiberg bond orders[17] were calculated using the Natural Bond Orbital (NBO)[18] software at the level of optimization. The geometries of the optimized structures are drawn with CYLview.[19]

Model reaction: In accordance with Li's experiments,[7] $Rh_2(OAc)_4$ catalyzed carboxylation of 2-phenylphenol (**1a**) with CO_2 in the presence of the tricyclohexylphosphine (PCy_3) and additives of excessive ^{t}BuOK was used as the modelling reaction in the theoretical calculations (Scheme 3).

Scheme 3. Model reaction in theoretical calculations

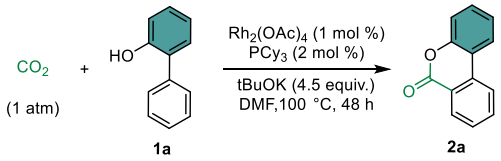

RESULTS AND DISCUSSION

The base of ^{t}BuOK could possibly react with CO_2 or phenate substrate (**1a**) to form potassium hemicarbonate (^{t}BuOCO$_2$K)[20] and potassium phenol (**1aK**). Both processes are thermodynamically feasible (Figure S2). Meanwhile, as to the initial state of the dimeric rhodium catalyst, $Rh_2(OAc)_4$ could possibly undergo the coordination of phosphine ligands (PCy_3), solvent (DMF), CO_2 or **1aK**. The results (Figure S3) demonstrate that the coordination of two equivalent PCy_3 is more feasible than all other cases, and thus the resultant **Rh0** (Figure 1) was chosen as the energy reference. From **Rh0**, ligand exchange of one PCy_3 with **1aK** occurs favorably via a dissociative pathway, including the elementary steps of dissociating one PCy_3 (**Rh0→Rh1**), ligand rearrangement (**Rh1→Rh2**), **1aK** coordination (**Rh2→Rh3**), and KOAc dissociation (**Rh3→Rh4**) steps. Of note, the other mechanistic possibility (such as rhodium dimer catalyst dissociation, ligand exchange between hemicarbonate and acetate *etc.*) were also examined, but was excluded due to the relatively higher energy demands (see Figure S4-5 for the details).

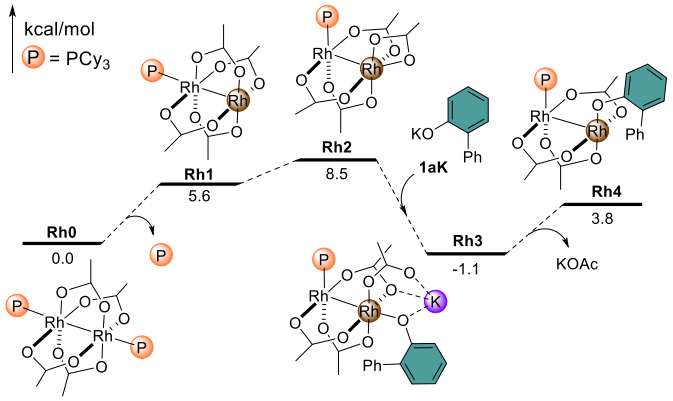

Figure 1. Gibbs free energy profiles of the ligand exchange steps from **Rh0**.

From **Rh4**, the C-H metalation step (i.e. C-H bond cleavage in Scheme 2) occurring via 1,2-addition,[21] or concerted metalation-deprotonation (CMD) pathways[22] were all taken into account (Figure 2, Figure S6-7). The calculation results indicate that the CMD mechanism with external base is the most feasible one (Figure 2). This pathway occurs via the coordination of potassium hemicarbonate (**Rh4→Rh5**) and C-H bond cleavage (**Rh5→TS1→Rh6**) steps, corresponding to the external base mediated concerted metalation-deprotonation pathway. In **Rh6**, the bicarbonate is weakly ligated on the Rh-complex via electrostatic interaction, and the dissociation of the ^{t}BuOCO$_2$H moiety is thermodynamically favored by the entropic effect (**Rh6→Rh7**). After that, dissociation of one acetate group (in the form of KOAc) could possibly occur to generate the type **III** intermediate in Scheme 2 (note: acetate dissociation on earlier intermediates **Rh1**/**Rh2**/**Rh4** are unlikely, see Figure S8 for details). According to the calculation results, the dissociation of trans-acetate (refer to the remaining phosphine ligand, in the form of KOAc) is remarkably more favorable compared to that of the cis-one (**Rh8** vs **Rh8'**). Herein, it is noteworthy that the 2-phenylphenol group in **Rh8** undergoes a spontaneous rearrangement after the removal of the KOAc group, and the partial optimization and molecular dynamics analysis have confirmed that the rearrangement is spontaneously carried out in the reaction system (Figure S9-10). The high energy of **Rh8'** (39.5 kcal/mol) excludes its formation under the experimental condition (90-100 °C),[7] and thus the subsequent transformation on **Rh8'** is omitted.

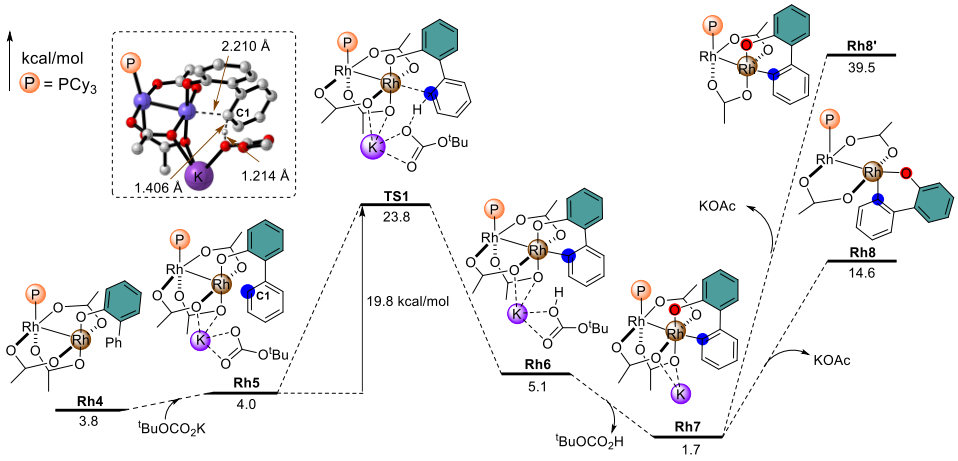

Figure 2. Gibbs free energy profiles of the C-H bond cleavage steps.

From **Rh8**, the carboxylation (i.e. CO_2 insertion) could occur on either Rh-O or Rh-C bond. As shown in Figure 3, the Rh-O bond insertion starts with approaching of CO_2 to the phenolic hydroxyl group, and this process is slightly endergonic by 2.8 kcal/mol. From the formed intermediate **Rh9**, a concerted Rh-O and O-C bond formation occurs via the transition state **TS2** to form the carboxylate intermediate **Rh10**. Although the energy barrier of the elementary Rh-O insertion step is only 16.3 kcal/mol, the relatively high energy of **TS2** compared to the energy reference excludes such mechanistic possibility. Meanwhile, the Rh-C insertion is less feasible than the Rh-O bond from both kinetic and thermodynamic aspects. To this end, the direct carboxylation on the intermediate **Rh8** could be rule out, and the main difficulty lies in the highly endergonic OAc-dissociating step (**Rh7→Rh8**). Motivated by this assumption, we examined the possibility for carboxylation without removing the OAc^- group. Specifically, in view of the nucleophilic carboxylation step, removing K^+ was also anticipated to be favorable due to the formation of an anionic, more nucleophilic Rh_2 catalyst (compared to the neutral one).

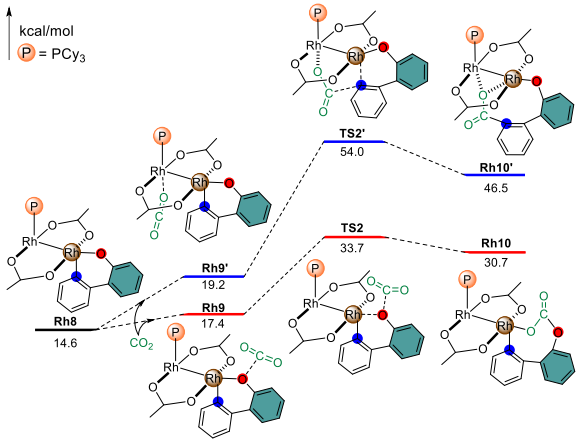

Figure 3. Gibbs free energy profiles of the acetate dissociation and carboxylation steps.

According to the calculation results, the relative energy of the supposed intermediate **Rh11** is 3.4 kcal/mol lower than that of **Rh7** (note: an isodesmic reaction was designed via incorporating of another $^tBuOCO_2K$ molecule). From **Rh11**, either a direct carboxylation pathway or a dissociation-carboxylation pathway (via dissociating the Rh^1-O^1 bond prior to the carboxylation step, Figure 4)

were examined. In view of the coordination environment of the Rh^1 center, these two pathways formally correspond to the outer-sphere or inner-sphere carboxylation mechanism, respectively. The outer-sphere pathway starts with the approaching of CO_2 into the Rh-O or Rh-C bond to form the intermediate **Rh15** or **Rh15'**, from which the occurs then to generate the metallacycle intermediate **Rh14** or **Rh14'**. All efforts in locating the Rh-O carboxylation transition state were failed, and the partial optimization by fixing $C(CO_2)$-O^1 bond at different distances indicated an energy demands of ~23.2 kcal/mol (Figure S11). On the other hand, the Rh-C carboxylation occurs via the transition state **TS4'**, with an energy barrier of 28.7 kcal/mol. Comparing the two outer-sphere pathways, the Rh-O carboxylation is kinetically more feasible, while the Rh-C carboxylation is thermodynamically more feasible. Similar to the results on the outer-sphere pathways, the inner-sphere Rh-O and Rh-C carboxylation are thermodynamically and kinetically favored, respectively. But the overall energy barrier is relatively higher than the related outer-sphere one (**TS3** vs **Scan-TS4**; **TS3'** vs **TS4'**), and therefore such mechanistic possibilities could be excluded. In this context, both **Rh14** and **Rh14'** are the possible product of the carboxylation step, and therefore we further examined the following lactonization mechanism on these two intermediates.

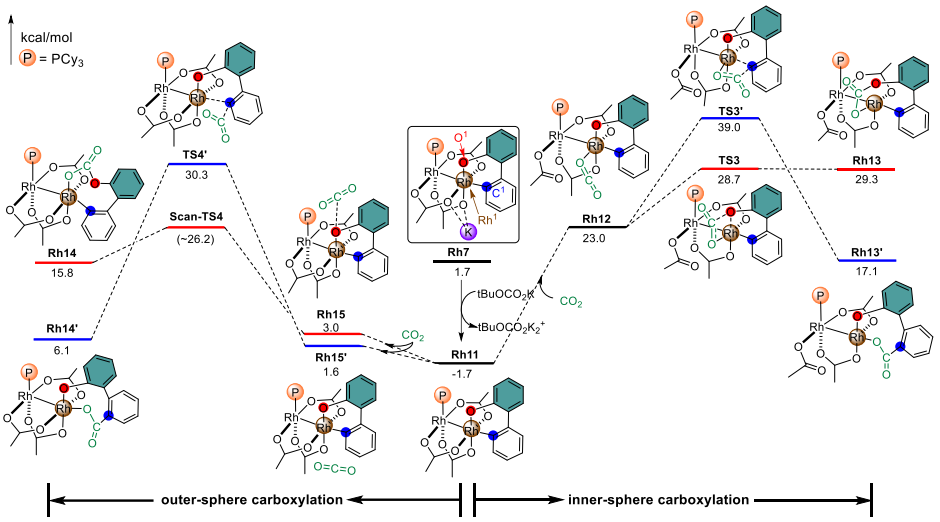

Figure 4. Gibbs free energy profiles of the carboxylation without acetate dissociation.

From **Rh14** and **Rh14'**, lactonization may occur via different pathways. For clarity reasons, an illustrative diagram on the direct cyclization or CO_2-assisted cyclization[23] is given in Scheme 3. In addition, the mechanism with protonation of the anionic intermediates occurring before the lactonization may also occur. The calculation results indicate that the direct cyclization pathway needs to overcome the high energy barrier of > 36 kcal/mol (Figures S12). Meanwhile, the CO_2-assisted cyclization is relatively more feasible than the direct lactonization pathway, but all these pathways need to overcome high total energy demand of > 38 kcal/mol, which is inaccessible in the target reaction system (Figure S13-15).

Scheme 3. Possible strategies for the lactonization process

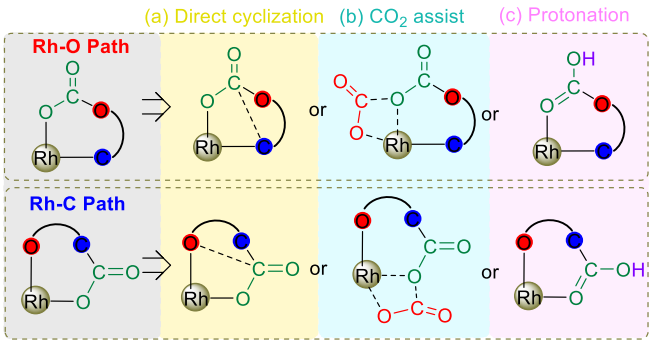

It was noticed that along with the formation of **1aK** and the C-H bond activation steps, alcohol or bicarbonate will be accumulated. We wondered whether these proton donators could undergo a proton transfer pathway with the rhodium anion species, thereby promoting the subsequent lactonization process. When experiencing the Rh-O carboxylation, the energy of the subsequent transformation step from **Rh14** is still too high to carry out (Figure S16). For the Rh-C carboxylation, the process from **Rh14'** to **Rh16** via proton transfer is more feasible. Furthermore, **Rh16** could afford the four-membered metallacycle species **Rh17**, and the energy barrier of this step is 10.3 kcal/mol (Figure 5). With the dissociation of O^1 atom from Rh^1, **Rh17** is transformed into **Rh17'**. Then, the **Rh18** and **Rh18'** are obtained with the O^3-Rh^1 coordination via the anti- and syn-pathway, respectively (note: anti- and syn- refer to the orientation of hydroxyl and phosphine ligands moiety). The hydroxyl-coordinated intermediates **Rh19** (anti-pathway) and **Rh19'** (syn-pathway) can be obtained logically by C-O^3 bond cleavage. Obviously, syn-pathway is more advantageous dynamically and thermodynamically, so we follow up on the conversion of **Rh19'**.

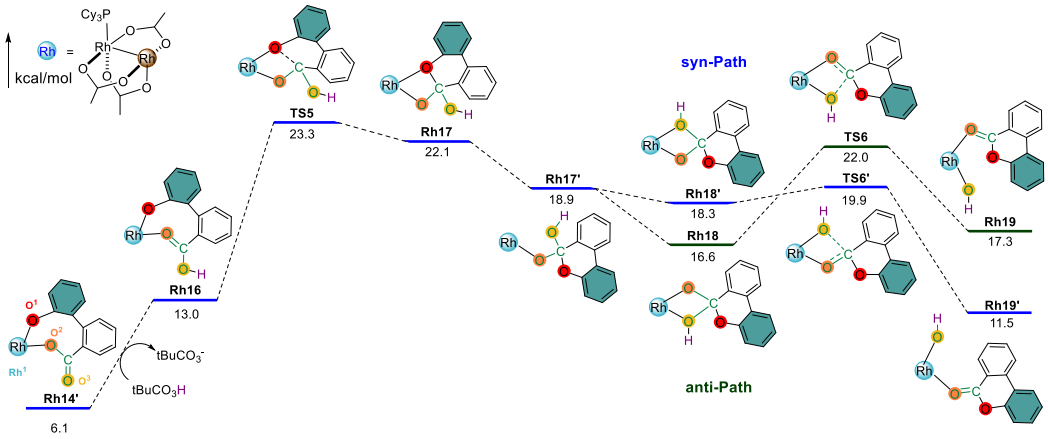

Figure 5. Gibbs free energy profiles of the lactonization after **Rh14'** protonation.

Regarding the regeneration of the rhodium catalyst, we proposed the following CO_2-assisted conversion (Figure 6). After obtained the **Rh19'**, potassium phenolate (**1aK**) can easily replace the lactone (**2a**) to produce **Rh21** accompanied by the exotherm of 16.7 kcal/mol, which is more advantageous than directly escaping **2a** and generating **Rh20**. Subsequently, CO_2 is inserted into the K-O (hydroxyl) bond to provide **Rh22** ($\Delta G^{\neq}$ = 10.2 kcal/mol), which is superior to the direct dehydrogenation (**Rh21**→**Rh4**, ΔG^{r} = 24.3 kcal/mol). With the subsequent $KHCO_3$ dissociation of **Rh22**, intermediate **Rh4** is regenerated and thus realizing the catalytic cycle.

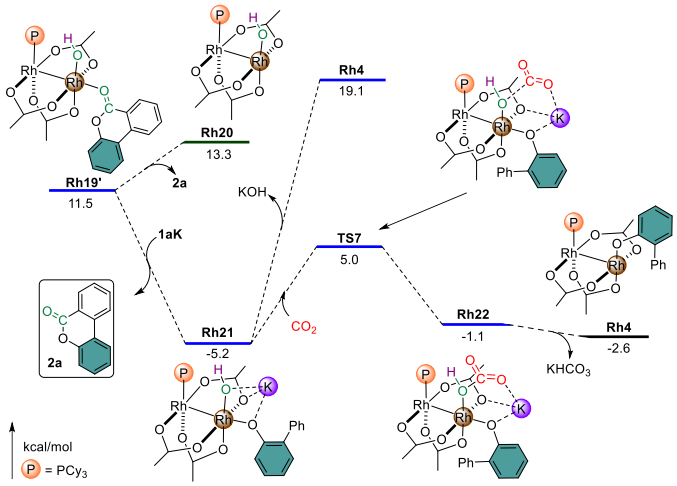

Figure 6. Gibbs free energy profiles of CO_2-assisted catalyst regeneration.

In addition to the aforementioned C-H activation-carboxylation mechanism, we also probed the plausibility of the carboxylation-C-H bond activation mechanism. As shown in Figure 7, the potassium phenate substrate (**1aK**) complexed with CO_2 could achieve the carboxylation species (**1aK'**), and coordinated with **Rh2** to form **Rh23** subsequently. This scheme is dominated compared with the route of CO_2 insertion into the **Rh4** intermediate (Figure S17). As potassium acetate dissociates (**Rh23**→**Rh24**), ^{t}BuOCO$_2$K mediated concerted metalation-deprotonation can get the corresponding metallacycle species **Rh26** ($\Delta G^{\neq}$ = 23.4 kcal/mol). Unfortunately, the high energy of **Rh25** made the C-H activation need to overcome a total energy barrier of 41.0 kcal/mol, which prevented the implementation of the strategy.

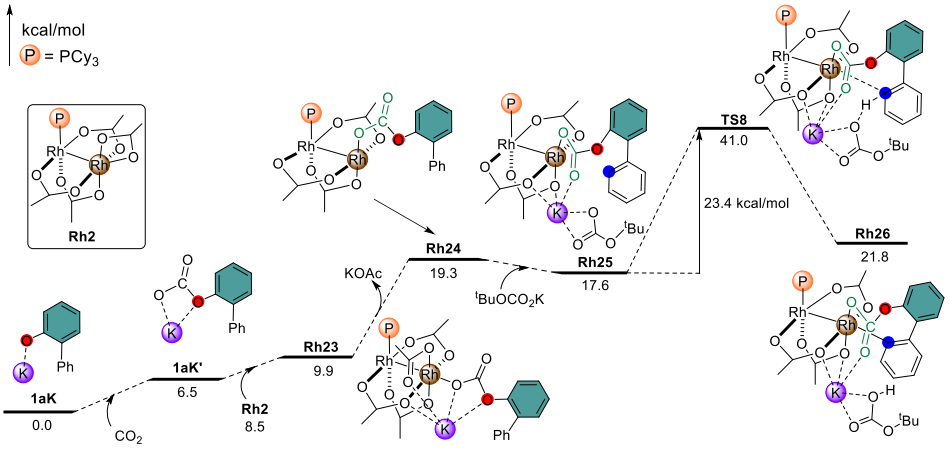

Figure 7. Gibbs free energy profiles of the carboxylation-first path.

We have noticed that the base has played an irreplaceable role in the reaction system (i.e. the activation of the C-H bond and the protonation step). Li's report pointed out that ^{t}BuOK, ^{t}BuOCO$_2$K, KOAc, $KHCO_3$ or K_2CO_3 may all be the existence of potassium salts,[7] while the specific types of potassium salts that assist the reaction is questionable. To clarify the "vital base" and the inherent difference of the various bases, we calculated and compared the auxiliary effects of the bases and the corresponding data were shown in Scheme 4. It is obvious that the energy barrier for C-H bond activation gradually increases with the alkalinity of the potassium salt decreases. Among them, ^{t}BuOCO$_2$K is the reasonable state that can take into account the steps of C-H bond activation and

protonation. Meanwhile, we found that there exists a robust linear relevance between the energy barrier ($\Delta G^{\neq}$) and reaction energy (ΔG^{r}) in the C-H bond activation step (Figure 8A). Therefore, the C-H bond acidity (usually measured by pKa) of the corresponding conjugate acid (denoted as **H-Base**) may be used as an efficacious parameter to evaluate the reaction energy barrier ($\Delta G^{\neq}$). As expected, a satisfactory linear correlation exists between pKa and $\Delta G^{\neq}$ (Figure 8B), which implies that the energy barrier of C-H bond activation can be predicted through the pKa of **H-Base**.

Scheme 4. Gibbs free energy data of C-H bond activation and protonation with various bases (part).

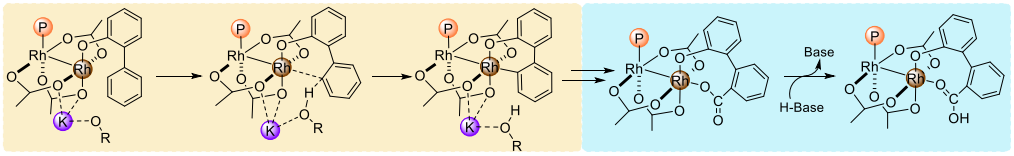

MOR (Base)	Rh5-MOR	TS1-MOR	Rh6-MOR	ΔG^{r}(C-H activation)	$\Delta G^{\neq}$	H-Base	ΔG^{r} (Protonation)	pKa (in DMF)
^{t}BuOK	2.6	11.1	-22.6	-25.2	8.5	^{t}BuOH	39.4	39.2
K_2CO_3	4.3	14.6	-17.3	-21.5	10.3	$KHCO_3$	34.8	35.1
KOAc	5.9	25.0	7.6	3.2	19.1	HOAc	12.8	21.9
^{t}BuOCO$_2$K	**4.0**	**23.8**	**5.1**	**1.1**	**19.8**	**^{t}BuOCO$_2$H**	**7.0**	**18.3**
$KHCO_3$	6.4	28.2	12.8	6.4	21.8	H_2CO_3	4.9	17.2

To gain detailed insights into the nature of the C−H activation transition state, especially to determine whether the deprotonation has really undergone a fully concerted metalation-deprotonation (CMD) fashion, or just a base-assisted internal electrophilic substitution-type (BIES) mechanism (more recently also abbreviated as eCMD),[24] a framework of More O'Ferrall-Jencks plot[25] was taken out as a reference (see SI for more details).[26] The introduction of strong base adjuvants resulted in smaller Rh-C bond orders, and all of the transition states located at the left-hand site of the plot and into the CMD regime (Figure 9), which is consistent with our previous conjecture.

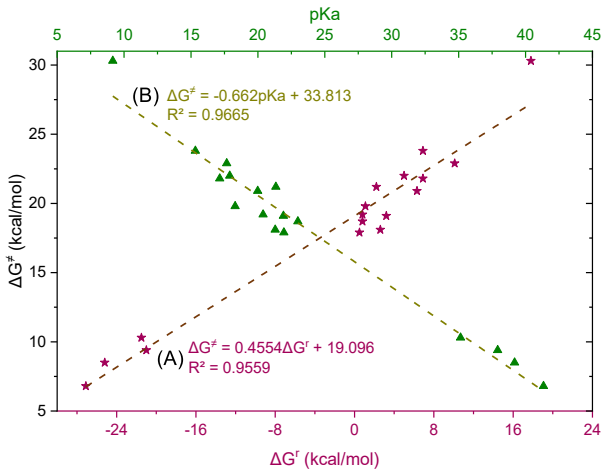

Figure 8. Comparison of reaction energy (ΔG^{r}) and pKa versus energy barrier ($\Delta G^{\neq}$) in the Rh-catalyzed C-H bond activation steps

Aside from the C-H activation, the **H-Base** also contributes to the protonation step of the carboxylate product, which is pivotal to the lactonization processes (Figure 5). As the acidity of **H-**

Base increases, the reaction energy of the protonation process gradually decreases. Since the protonation process is essentially the dissociation process of conjugate acid, thus the phenomenon is understandable. According to the previous steps, the alkalinity of the **Base** should be sufficiently strong to promote the C-H bond cleavage of **Rh5**; simultaneously, the acidity of the **H-Base** should be adequately strong to deliver proton to **Rh14'**. In other words, the alkalinity of the auxiliary base should be moderate.

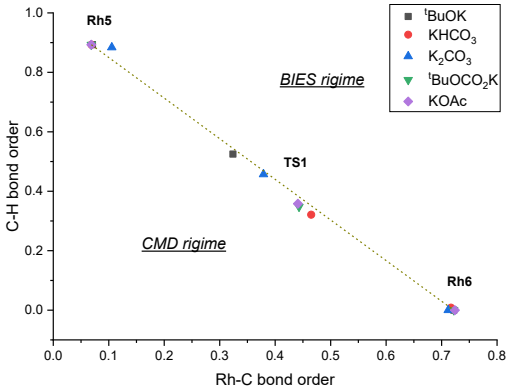

Figure 9. Wiberg bond order analysis of C−H bond activation for distinct rhodium complexes

We also paid attention to the other ligands mentioned by Li et al.,[7] for the ligands have played a vital role in the system. The energy data of corresponding key intermediates and transition states are shown in Figure 10. The C-H bond activation step is relatively easy, and the carboxylation step is still the rate-determining step. In particular, the total reaction energy barrier of corresponding ligands can correspond well to the reaction temperature and yield given by Li et al.,[7] which also confirms the rationality of the computational mechanism path. The distortion/interaction model analysis[27] was carried out to explore the causes of Rh-C carboxylation (Figure S18), and the results indicate that the distortion energy dominates the energy barrier of the carboxylation step.

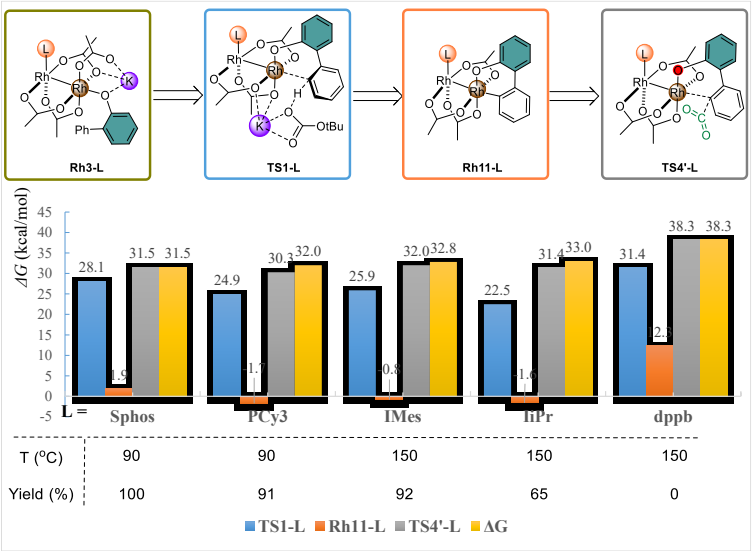

Figure 10. The relative energies chart of critical intermediates and transition states with different ligands (**Rh3-L** as the reference point)

CONCLUSION

The rhodium-catalyzed aryl C-H bond carboxylation with CO_2 uncovers a truly novel site selectivity to generate high value-added chemicals. In this paper, the mechanical details on the C-H bond activation, the site selectivity of carboxylation, and lactonization by rhodium dimer catalysis were explored through DFT calculations. The role of the base in the C-H bond activation step was revealed clearly, and the alkalinity determines the energy barrier of activation. In the carboxylation step, CO_2 can be inserted into the Rh-O and Rh-C bond kinetically and thermodynamically, respectively. In the process of lactonization, the fascinating results hint at the critical role of conjugate acid and CO_2: to carry out the protonation and regenerate the rhodium catalyst, respectively. As for the carboxylation-first pathway, the instability of the carboxylated intermediate hinders the subsequent C-H bond activation process. All in all, these discoveries could have great guiding significance for developing related types of reactions.

Conflicts of interest

The authors declare no competing interests.

Acknowledgements

We are grateful for the support from National Natural Science Foundation of China (21732006, 51821006, 51961135104).

Notes and references

1. (a) K. Huang, C. L. Sun and Z. J. Shi, Transition-metal-catalyzed C-C bond formation through the fixation of carbon dioxide, *Chem. Soc. Rev.*, 2011, **40**, 2435-2452; (b) Q. Liu, L. Wu, R. Jackstell and M. Beller, Using carbon dioxide as a building block in organic synthesis, *Nat Commun*, 2015, **6**, 5933; (c) K. Sekine and T. Yamada, Silver-catalyzed carboxylation, *Chem. Soc. Rev.*, 2016, **45**, 4524-4532; (d) M. Borjesson, T. Moragas, D. Gallego and R. Martin, Metal-Catalyzed Carboxylation of Organic (Pseudo)halides with CO2, *ACS Catal*, 2016, **6**, 6739-6749; (e) Z. Zhang, J.-H. Ye, T. Ju, L.-L. Liao, H. Huang, Y.-Y. Gui, W.-J. Zhou and D.-G. Yu, Visible-Light-Driven Catalytic Reductive Carboxylation with CO2, *ACS Catal.*, 2020, **10**, 10871-10885; (f) X. W. Chen, J. P. Yue, K. Wang, Y. Y. Gui, Y. N. Niu, J. Liu, C. K. Ran, W. Kong, W. J. Zhou and D. G. Yu, Nickel-Catalyzed Asymmetric Reductive Carbo-Carboxylation of Alkenes with CO2, *Angew. Chem. Int. Ed.*, 2021, **60**, 14068-14075.
2. (a) T. Suga, H. Mizuno, J. Takaya and N. Iwasawa, Direct carboxylation of simple arenes with CO2 through a rhodium-catalyzed C-H bond activation, *Chem. Commun.*, 2014, **50**, 14360-14363; (b) N. Ishida, Y. Masuda, S. Uemoto and M. Murakami, A Light/Ketone/Copper System for Carboxylation of Allylic C-H Bonds of Alkenes with CO2, *Chem.-Eur. J.*, 2016, **22**, 6524-6527; (c) J. Luo and I. Larrosa, C-H Carboxylation of Aromatic Compounds through CO2 Fixation, *Chemsuschem*, 2017, **10**, 3317-3332; (d) Y. Gao, Z. Cai, S. Li and G. Li, Rhodium(I)-Catalyzed Aryl C-H Carboxylation of 2-Arylanilines with CO2, *Org. Lett.*, 2019, **21**, 3663-3669; (e) T. Saitou, Y. Jin, K. Isobe, T. Suga, J. Takaya and N. Iwasawa, Rh-Catalyzed Direct Carboxylation of Alkenyl C-H Bonds of Alkenylpyrazoles, *Chem. Asian J.*, 2020, **15**, 1941-1944; (f) C. Pei, J. Zong, S. Han, B. Li and B. Wang, Ni-Catalyzed Direct Carboxylation of an

Unactivated C-H Bond with CO2, *Org. Lett.*, 2020, **22**, 6897-6902.

3. (a) A. Correa and R. Martin, Palladium-catalyzed direct carboxylation of aryl bromides with carbon dioxide, *J. Am. Chem. Soc.*, 2009, **131**, 15974-15975; (b) H. Mizuno, J. Takaya and N. Iwasawa, Rhodium(I)-Catalyzed Direct Carboxylation of Arenes with CO2 via Chelation-Assisted C-H Bond Activation, *J. Am. Chem. Soc.*, 2011, **133**, 1251-1253; (c) T. Fujihara, K. Nogi, T. Xu, J. Terao and Y. Tsuji, Nickel-catalyzed carboxylation of aryl and vinyl chlorides employing carbon dioxide, *J. Am. Chem. Soc.*, 2012, **134**, 9106-9109; (d) K. Shimomaki, K. Murata, R. Martin and N. Iwasawa, Visible-Light-Driven Carboxylation of Aryl Halides by the Combined Use of Palladium and Photoredox Catalysts, *J. Am. Chem. Soc.*, 2017, **139**, 9467-9470.
4. (a) C. S. Yeung and V. M. Dong, Beyond Aresta's complex: Ni- and Pd-catalyzed organozinc coupling with CO2, *J. Am. Chem. Soc.*, 2008, **130**, 7826-7827; (b) Y. Makida, E. Marelli, A. M. Z. Slawin and S. P. Nolan, Nickel-catalysed carboxylation of organoboronates, *Chem. Commun.*, 2014, **50**, 8010-8013; (c) J. B. Diccianni, C. T. Hu and T. Diao, Insertion of CO2 Mediated by a (Xantphos)Ni(I) -Alkyl Species, *Angew. Chem. Int. Ed.*, 2019, **58**, 13865-13868; (d) A. Gevorgyan, K. H. Hopmann and A. Bayer, Formal C−H Carboxylation of Unactivated Arenes, *Chem.-Eur. J.*, 2020, **26**, 6064-6069.
5. (a) A. S. Lindsey and H. Jeskey, THE KOLBE-SCHMITT REACTION, *Chem. Rev.*, 1957, **57**, 583-620; (b) J. Luo, S. Preciado, P. Xie and I. Larrosa, Carboxylation of Phenols with CO2 at Atmospheric Pressure, *Chem.-Eur. J.*, 2016, **22**, 6798-6802; (c) Y. Sadamitsu, A. Okumura, K. Saito and T. Yamada, Kolbe-Schmitt type reaction under ambient conditions mediated by an organic base, *Chem. Commun.*, 2019, **55**, 9837-9840.
6. (a) M. Konno, M. Chiba, K. Nemoto and T. Hattori, Electrophilic Aromatic Substitution of Arenes with CO2 Mediated by R3SiB(C6F5)4, *Chem. Lett.*, 2012, **41**, 913-914; (b) A. N. Sarve, P. A. Ganeshpure and P. Munshi, Carboxylation of Toluene by CO2 Generating p-Toluic Acid: A Kinetic Look, *Ind. Eng. Chem. Res.*, 2012, **51**, 5174-5180; (c) S. Tanaka, M. Chiba, Y. Saito, T. Yamamoto and T. Hattori, AlBr3-Mediated Tandem Cyclization–Carboxylation of Allenylbenzenes with CO2 in the Presence of Pyridines, *Bull. Chem. Soc. Jpn.*, 2017, **90**, 419-421.
7. L. Fu, S. Li, Z. Cai, Y. Ding, X.-Q. Guo, L.-P. Zhou, D. Yuan, Q.-F. Sun and G. Li, Ligand-enabled site-selectivity in a versatile rhodium(ii)-catalysed aryl C–H carboxylation with CO2, *Nat. Catal.*, 2018, **1**, 469-478.
8. M. J. T. Frisch, G. W.; Schlegel, H. B.; Scuseria, G. E.; Robb, M. A.; Cheeseman, J. R.; Scalmani, G.; Barone, V.; Mennucci, B.; Petersson, G. A.; Nakatsuji, H.; Caricato, M.; Li, X.; Hratchian, H. P.; Izmaylov, A. F.; Bloino, J.; Zheng, G.; Sonnenberg, J. L.; Hada, M.; Ehara, M.; Toyota, K.; Fukuda, R.; Hasegawa, J.; Ishida, M.; Nakajima, T.; Honda, Y.; Kitao, O.; Nakai, H.; Vreven, T.; Montgomery, J. A., Jr.; Peralta, J. E.; Ogliaro, F.; Bearpark, M.; Heyd, J. J.; Brothers, E.; Kudin, K. N.; Staroverov, V. N.; Kobayashi, R.; Normand, J.; Raghavachari, K.; Rendell, A.; Burant, J. C.; Iyengar, S. S.; Tomasi, J.; Cossi, M.; Rega, N.; Millam, J. M.; Klene, M.; Knox, J. E.; Cross, J. B.; Bakken, V.; Adamo, C.; Jaramillo, J.; Gomperts, R.; Stratmann, R. E.; Yazyev, O.; Austin, A. J.; Cammi, R.; Pomelli, C.; Ochterski, J. W.; Martin, R. L.; Morokuma, K.; Zakrzewski, V. G.; Voth, G. A.; Salvador, P.; Dannenberg, J. J.; Dapprich, S.; Daniels, A. D.; Farkas, O.; Foresman, J. B.; Ortiz, J. V.; Cioslowski, J.; Fox, D. J.; , Gaussian 16, revision C.01; Gaussian Inc.: Wallingford, CT, 2016.

9. (a) S. H. Vosko, L. Wilk and M. Nusair, Accurate spin-dependent electron liquid correlation energies for local spin density calculations: a critical analysis, *Can. J. Phys.*, 1980, **58**, 1200-1211; (b) C. Lee, W. Yang and R. G. Parr, Development of the Colle-Salvetti correlation-energy formula into a functional of the electron density, *Phys Rev B Condens Matter*, 1988, **37**, 785-789; (c) A. D. Becke, Density‐functional thermochemistry. III. The role of exact exchange, *J. Chem. Phys.*, 1993, **98**, 5648-5652; (d) P. J. Stephens, F. J. Devlin, C. F. Chabalowski and M. J. Frisch, Ab Initio Calculation of Vibrational Absorption and Circular Dichroism Spectra Using Density Functional Force Fields, *J. Phys. Chem.*, 1994, **98**, 11623-11627.
10. (a) S. Grimme, J. Antony, S. Ehrlich and H. Krieg, A consistent and accurate ab initio parametrization of density functional dispersion correction (DFT-D) for the 94 elements H-Pu, *J. Chem. Phys.*, 2010, **132**, 154104; (b) S. Grimme, S. Ehrlich and L. Goerigk, Effect of the damping function in dispersion corrected density functional theory, *J. Comput. Chem.*, 2011, **32**, 1456-1465.
11. (a) Y. Kataoka, Y. Kitagawa, T. Saito, Y. Nakanishi, T. Matsui, K. Sato, Y. Miyazaki, T. Kawakami, M. Okumura, W. Mori and K. Yamaguchi, Theoretical Study on the Electronic Configurations and Nature of Chemical Bonds of Dirhodium Tetraacetato Complexes [Rh2(CH3COO)4(L)2] (L = H2O, Free): Broken Symmetry Approach, *Bull. Chem. Soc. Jpn.*, 2010, **83**, 1481-1488; (b) Z. J. Garlets, J. N. Sanders, H. Malik, C. Gampe, K. N. Houk and H. M. L. Davies, Enantioselective C-H functionalization of bicyclo 1.1.1 pentanes, *Nat. Catal.*, 2020, **3**, 351-357; (c) Y. Li, Y. T. Zhao, T. Zhou, M. Q. Chen, Y. P. Li, M. Y. Huang, Z. C. Xu, S. F. Zhu and Q. L. Zhou, Highly Enantioselective O-H Bond Insertion Reaction of alpha-Alkyl- and alpha-Alkenyl-alpha-diazoacetates with Water, *J. Am. Chem. Soc.*, 2020, **142**, 10557-10566.
12. D. Andrae, U. Häußermann, M. Dolg, H. Stoll and H. Preuß, Energy-adjustedab initio pseudopotentials for the second and third row transition elements, *Theor. Chim. Acta.*, 1990, **77**, 123-141.
13. (a) R. Ditchfield, W. J. Hehre and J. A. Pople, Self‐Consistent Molecular‐Orbital Methods. IX. An Extended Gaussian‐Type Basis for Molecular‐Orbital Studies of Organic Molecules, *J. Chem. Phys.*, 1971, **54**, 724-728; (b) W. J. Hehre, R. Ditchfield and J. A. Pople, Self—Consistent Molecular Orbital Methods. XII. Further Extensions of Gaussian—Type Basis Sets for Use in Molecular Orbital Studies of Organic Molecules, *J. Chem. Phys.*, 1972, **56**, 2257-2261; (c) P. C. Hariharan and J. A. Pople, The influence of polarization functions on molecular orbital hydrogenation energies, *Theor. Chim. Acta.*, 1973, **28**, 213-222.
14. (a) Y. Zhao and D. G. Truhlar, Density functionals with broad applicability in chemistry, *Acc. Chem. Res.*, 2008, **41**, 157-167; (b) Y. Zhao and D. G. Truhlar, The M06 suite of density functionals for main group thermochemistry, thermochemical kinetics, noncovalent interactions, excited states, and transition elements: two new functionals and systematic testing of four M06-class functionals and 12 other functionals, *Theor. Chem. Acc.*, 2008, **120**, 215-241.
15. A. V. Marenich, C. J. Cramer and D. G. Truhlar, Universal solvation model based on solute electron density and on a continuum model of the solvent defined by the bulk dielectric constant and atomic surface tensions, *J. Phys. Chem. B*, 2009, **113**, 6378-6396.
16. (a) K. Fukui, Formulation of the reaction coordinate, *J. Phys. Chem.*, 1970, **74**, 4161-4163; (b) K. Fukui, The path of chemical reactions - the IRC approach, *Acc. Chem. Res.*, 1981, **14**, 363-368.
17. K. B. Wiberg, Application of the pople-santry-segal CNDO method to the cyclopropylcarbinyl

and cyclobutyl cation and to bicyclobutane, *Tetrahedron*, 1968, **24**, 1083-1096.

18. (a) J. P. Foster and F. Weinhold, Natural hybrid orbitals, *J. Am. Chem. Soc.*, 1980, **102**, 7211-7218; (b) A. E. Reed and F. Weinhold, Natural bond orbital analysis of near‐Hartree‐Fock water dimer, *J. Chem. Phys.*, 1983, **78**, 4066-4073; (c) A. E. Reed, R. B. Weinstock and F. Weinhold, Natural population analysis, *J. Chem. Phys.*, 1985, **83**, 735-746.
19. CYLview, 1.0b, C. Y. Legault, Université de Sherbrooke, 2009 (http://www.cylview.org).
20. B. M. Pope and P. BM, DI-TERT-BUTYL DICARBONATE, *Org. Syn.*, 1977, **57**, 45–50.
21. D. Balcells, E. Clot and O. Eisenstein, C—H Bond Activation in Transition Metal Species from a Computational Perspective, *Chem. Rev.*, 2010, **110**, 749-823.
22. (a) L. David and F. Keith, Overview of the Mechanistic Work on the Concerted Metallation–Deprotonation Pathway, *Chem. Lett.*, 2010, **39**, 1118-1126; (b) Y.-F. Yang and Y. She, Computational exploration of Pd-catalyzed C-H bond activation reactions, *Int. J. Quantum Chem*, 2018, **118**.
23. L. Song, L. Zhu, Z. Zhang, J. H. Ye, S. S. Yang, J. L. Han, Z. B. Yin, Y. Lan and D. G. Yu, Catalytic Lactonization of Unactivated Aryl C-H Bonds with CO2: Experimental and Computational Investigation, *Org. Lett.*, 2018, **20**, 3776-3779.
24. (a) D. Zell, M. Bursch, V. Müller, S. Grimme and L. Ackermann, Full Selectivity Control in Cobalt(III)-Catalyzed C−H Alkylations by Switching of the C−H Activation Mechanism, *Angew. Chem. Int. Ed.*, 2017, **56**, 10378-10382; (b) K. Naksomboon, J. Poater, F. M. Bickelhaupt and M. A. Fernandez-Ibanez, para-Selective C-H Olefination of Aniline Derivatives via Pd/S,O-Ligand Catalysis, *J. Am. Chem. Soc.*, 2019, **141**, 6719-6725; (c) L. Wang and B. P. Carrow, Oligothiophene Synthesis by a General C–H Activation Mechanism: Electrophilic Concerted Metalation–Deprotonation (eCMD), *ACS Catal.*, 2019, **9**, 6821-6836.
25. (a) R. A. M. O'Ferrall, Relationships between E2 and E1cB mechanisms of β-elimination, *J. Chem. Soc. B*, 1970, **0**, 274-277; (b) W. P. Jencks, General acid-base catalysis of complex reactions in water, *Chem. Rev.*, 1972, **72**, 705-718.
26. T. Rogge, J. C. A. Oliveira, R. Kuniyil, L. Hu and L. Ackermann, Reactivity-Controlling Factors in Carboxylate-Assisted C–H Activation under 4d and 3d Transition Metal Catalysis, *ACS Catal.*, 2020, **10**, 10551-10558.
27. (a) F. Liu, R. S. Paton, S. Kim, Y. Liang and K. N. Houk, Diels-Alder Reactivities of Strained and Unstrained Cycloalkenes with Normal and Inverse-Electron-Demand Dienes: Activation Barriers and Distortion/Interaction Analysis, *J. Am. Chem. Soc.*, 2013, **135**, 15642-15649; (b) S. M. Chen, X. Q. Huang, E. Meggers and K. N. Houk, Origins of Enantioselectivity in Asymmetric Radical Additions to Octahedral Chiral-at-Rhodium Enolates: A Computational Study, *J. Am. Chem. Soc.*, 2017, **139**, 17902-17907.